

# ZrB<sub>2</sub>–ZrC<sub>x</sub>N<sub>1–x</sub> Eutectic Composites Produced by Melt Solidification

Eric Jianfeng Cheng,<sup>‡,§,†</sup> Hirokazu Katsui,<sup>‡</sup> and Takashi Goto<sup>‡,†</sup>

<sup>‡</sup>Institute for Materials Research, Tohoku University, 2-1-1, Katahira, Aoba-ku, Sendai 980-8577, Japan

<sup>§</sup>Department of Mechanical Engineering, University of Michigan, 2350 Hayward, G.G. Brown Laboratory, Ann Arbor, Michigan 48109

Ceramic eutectics are naturally occurring *in-situ* composites and can offer superior mechanical properties. Here, ZrB<sub>2</sub>–ZrC<sub>x</sub>N<sub>1–x</sub> quasi-binary ceramic eutectic composites were produced by arc-melting a mixture of ZrB<sub>2</sub>, ZrC, and ZrN powders in an N<sub>2</sub> atmosphere. The arc-melted ZrB<sub>2</sub>–ZrC<sub>x</sub>N<sub>1–x</sub> composites containing 50 mol% of ZrB<sub>2</sub> (irrespective of the ZrC/ZrN ratio) showed rod-like eutectic structures, where ZrC<sub>x</sub>N<sub>1–x</sub> single-crystalline rods were dispersed in the ZrB<sub>2</sub> single-crystalline matrices. Multiple orientation relationships between the ZrC<sub>x</sub>N<sub>1–x</sub> rods and the ZrB<sub>2</sub> matrices were observed, and one was determined as ZrB<sub>2</sub> {0110} // ZrC<sub>x</sub>N<sub>1–x</sub> {111} and ZrB<sub>2</sub> <2110> // ZrC<sub>x</sub>N<sub>1–x</sub> <101>. The rod-like eutectic composites had higher hardness than the hypo- and hypereutectic composites and the 50ZrB<sub>2</sub>–40ZrC–10ZrN (mol%) eutectic composite showed the highest Vickers hardness (*H<sub>v</sub>*) of 19 GPa.

## I. Introduction

ZrB<sub>2</sub>, ZrC, and ZrN are members of a family of materials known as ultra high-temperature ceramics (UHTCs).<sup>1</sup> The melting temperatures of ZrB<sub>2</sub>, ZrC, and ZrN are about 3520, 3970, and 3170 K, respectively.<sup>2</sup> Besides high melting temperatures, the Zr-based compounds also offer an excellent combination of chemical stability, high electrical and thermal conductivities, low density, and high thermal shock resistance.<sup>2–5</sup> As naturally occurring *in-situ* composites, ceramic eutectics can combine the properties of two or more components and possess superior mechanical properties, such as higher wear resistance and better fracture toughness, to the monolithic materials.<sup>6–9</sup> Sorrel et al. reported a directionally solidified ZrB<sub>2</sub>–ZrC lamellar eutectic composite, which showed higher hardness, higher fracture toughness, and better wear resistance than the monolithic ZrB<sub>2</sub> and ZrC.<sup>10</sup> Chen et al. synthesized a LaB<sub>2</sub>–ZrB<sub>2</sub> rod-like eutectic composite that exhibited higher hardness and fracture toughness in comparison with the individual components of LaB<sub>2</sub> and ZrB<sub>2</sub>.<sup>11</sup> Hence, the ZrB<sub>2</sub>–ZrC–ZrN ceramic composites could take the advantage of the physical and mechanical properties of ZrB<sub>2</sub>, ZrC, and ZrN, and would be promising materials for reentry and hypersonic vehicles, where resistance to corrosion, wear, and oxidation is demanded.<sup>4</sup>

ZrB<sub>2</sub> has a hexagonal crystal structure, while ZrC and ZrN share the same face-centered cubic crystal structures.<sup>1,2</sup> The ZrB<sub>2</sub>–ZrC and ZrB<sub>2</sub>–ZrN both are quasi-binary eutectic systems, and the ZrC–ZrN is a complete solid solution system of ZrC<sub>x</sub>N<sub>1–x</sub>.<sup>12–14</sup> Therefore, the ZrB<sub>2</sub>–ZrC–ZrN is

expected to be a quasi-binary eutectic system of ZrB<sub>2</sub>–ZrC<sub>x</sub>N<sub>1–x</sub>. By now, however, no research has been reported on the synthesis of ZrB<sub>2</sub>–ZrC<sub>x</sub>N<sub>1–x</sub> quasi-binary eutectic composites. A similar ternary system, TiB<sub>2</sub>–TiC–TiN, has been reported to be a quasi-binary eutectic system of TiB<sub>2</sub>–TiC<sub>x</sub>N<sub>1–x</sub>.<sup>15</sup>

Because of strong covalent bonding and low self-diffusion coefficients of elements in the transition-metal borides, carbides and nitrides, synthesis of these transition-metal-based ceramic composites with high density would require long exposures to high temperatures.<sup>16</sup> The melt-solidification process was useful for consolidating high-melting-point materials to produce fully dense composites.<sup>15,17</sup> In addition, self-assembled structures by eutectic reactions could improve the mechanical properties of the constituent materials.<sup>7,8</sup> In this study, *in-situ* ZrB<sub>2</sub>–ZrC–ZrN composites were produced by arc-melting a mixture of ZrB<sub>2</sub>, ZrC, and ZrN powders in an N<sub>2</sub> atmosphere, and the microstructures, mechanical properties and crystal orientation relationships between phases of the produced eutectic composites were investigated.

## II. Experimental Procedure

The starting materials used in this study were ZrB<sub>2</sub> powder (C < 0.50, O < 1.50, N < 0.50 (wt%), 1.5–2.5 μm, Kojundo Chemical Laboratory, Saitama, Japan), ZrC powder (95%, 2.5 μm, Kojundo Chemical Laboratory), and ZrN powder (98%, Kojundo Chemical Laboratory). The compositions in this study were expressed as nominal mole percentages of ZrB<sub>2</sub>, ZrC, and ZrN. The nominal compositions of the prepared composites are shown in Fig. 1, in which each dot corresponds to one nominal composition. The powders of ZrB<sub>2</sub>, ZrC, and ZrN were ball-milled with ZrO<sub>2</sub> balls in a small amount of ethanol, and ball-milled for 4 h in a polyethylene bottle. The mixed powders were dried at 333 K for 12 h, and isostatically pressed into disks (10 mm in diameter and 3 mm in thickness) under a pressure of 5 MPa. The pressed powder disks were melted twice by an arc-melting technique in an N<sub>2</sub> atmosphere at 80 kPa and solidified on a water-cooled copper hearth. N<sub>2</sub> gas was introduced to prevent the possible dissociation of ZrN during melting process. The specimens were polished with a series of diamond grits, with a final polish using a 1 μm diamond slurry. The crystallographic phases were examined using X-ray diffraction (XRD, Ultima IV; Rigaku, Tokyo, Japan) with CuKα radiation. The microstructures of the composites were investigated by scanning electron microscopy (SEM, Hitachi: S-3100H, Tokyo, Japan) at 10 kV and transmission electron microscopy (TEM, EM-002B; TOPCON, Tokyo, Japan). Electron probe microanalysis (EPMA) was carried out on an electron probe microanalyzer with a TSL solutions camera control system (JXA-8621MX, JEOL, Tokyo, Japan). Vickers hardness was determined from 10 indentation measurements. Crystal structure illustrations were produced using the VESTA software (Tohoku University, Sendai, Japan).<sup>18</sup>

E. Dickey—contributing editor

Manuscript No. 36834. Received May 4, 2015; approved September 11, 2015.

<sup>†</sup>Authors to whom correspondence should be addressed. e-mails: ericonium@gmail.com and goto@imr.tohoku.ac.jp

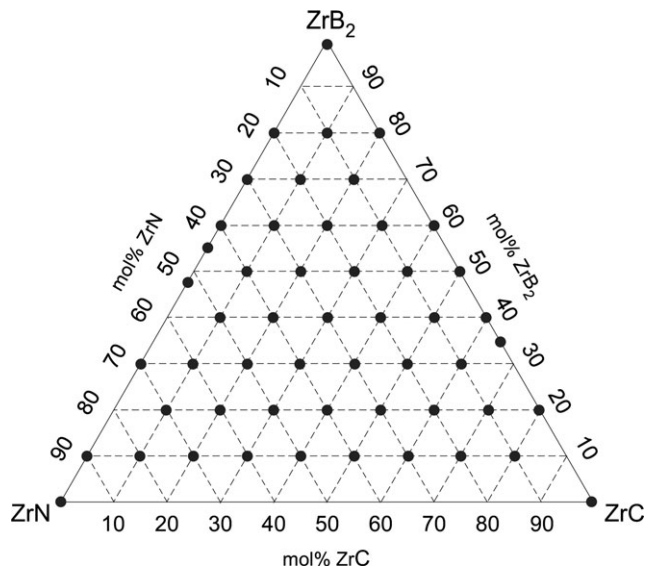


Fig. 1. Prepared nominal compositions (indicated by black dots) of mixtures of the  $ZrB_2$ ,  $ZrC$ , and  $ZrN$  starting powders.

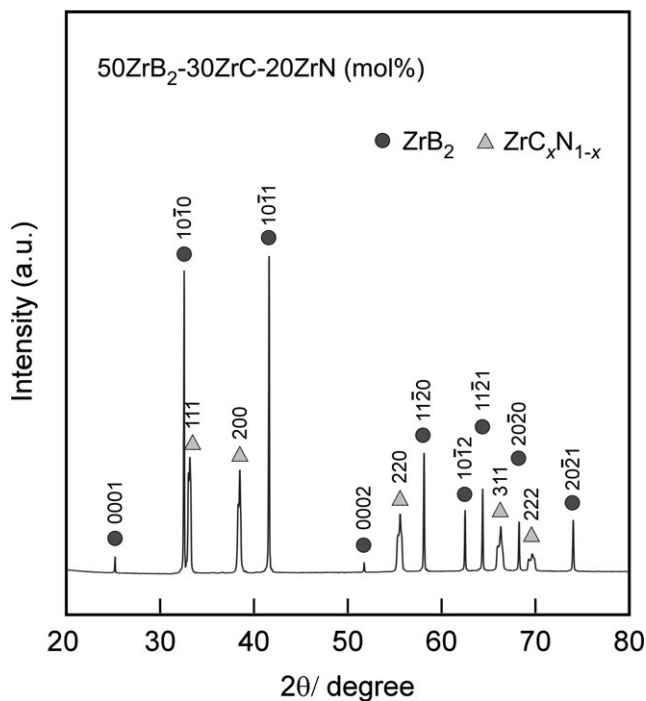


Fig. 2. XRD pattern of the arc-melted  $50ZrB_2-30ZrC-20ZrN$  (mol%) composite.

### III. Results and Discussion

Figure 2 shows the XRD pattern of the arc-melted  $50ZrB_2-30ZrC-20ZrN$  (mol%) composite. Reflection peaks relating to  $ZrB_2$  and  $ZrC_xN_{1-x}$  were observed, indicating that  $ZrC$ - and  $ZrN$ -formed solid solutions of  $ZrC_xN_{1-x}$ . Based on XRD results, only  $ZrB_2$  and  $ZrC_xN_{1-x}$  two phases were detected in all the arc-melted composites, irrespective of the  $ZrC$  and  $ZrN$  contents. Hence, the  $ZrB_2-ZrC-ZrN$  was a quasi-binary system, consisting of  $ZrB_2$  and  $ZrC_xN_{1-x}$  two phases.

Figure 3 presents the secondary electron SEM micrographs of the arc-melted  $ZrB_2-ZrC-ZrN$  composites, in which two phases are observed: the gray phase  $ZrC_xN_{1-x}$  and the black phase  $ZrB_2$ . For the nominal composition of  $30ZrB_2-50ZrC-20ZrN$  (mol%), the arc-melted  $ZrB_2-$

$ZrC_xN_{1-x}$  composite showed a hypoeutectic structure, comprising the dark-contrast  $ZrB_2$  phase and the gray-contrast primary  $ZrC_xN_{1-x}$  phase, as shown in Fig. 3(a). The composite of  $40ZrB_2-40ZrC-20ZrN$  (mol%) had a labyrinth-like eutectic structure [Fig. 3(b)]. With increasing  $ZrB_2$  content, elongated  $ZrB_2$  formed as the primary phase as shown in Figs. 3(c) and (d), and the two compositions of  $60ZrB_2-20ZrC-20ZrN$  and  $80ZrB_2-10ZrC-10ZrN$  (mol%) were hypereutectic. Rod-like eutectic structures were locally observed in Figs. 3(a) and (c).

On the other hand, the composites with nominal compositions of 50 mol% of  $ZrB_2$ , irrespective of the  $ZrC/ZrN$  (C/N) ratio, showed rod-like eutectic structures, where the gray  $ZrC_xN_{1-x}$  rods were uniformly dispersed in the black  $ZrB_2$  matrix, as shown in Fig. 4. As indicated by the dash-lined hexagon in Fig. 4(a), the  $ZrC_xN_{1-x}$  rods are hexagonally ordered. The diameter of the  $ZrC_xN_{1-x}$  rods slightly increased with increasing C/N ratio. Since  $ZrC$  had higher melting temperature (3970 K) than  $ZrN$  (3170 K), the melting temperature of  $ZrC_xN_{1-x}$  would be expected to increase with increasing C/N ratio. Consequently, the crystal growth rate of  $ZrC_xN_{1-x}$  would be affected, which could have resulted in the larger diameter of the  $ZrC_xN_{1-x}$  rods. The lattice parameter of  $ZrC$  (0.4691 nm) was larger than that of  $ZrN$  (0.4600 nm),<sup>19,20</sup> the lattice parameter of  $ZrC_xN_{1-x}$  would increase linearly with increasing C/N ratio. The change in the lattice parameter of  $ZrC_xN_{1-x}$  could be another factor associated with the change in the diameter of the  $ZrC_xN_{1-x}$  rods. The area ratio of the gray  $ZrC_xN_{1-x}$  phase in Fig. 4(d) was about 43% [that for Figs. 4(a)–(c) was 44%, 39%, and 42%, respectively], from which  $ZrC_xN_{1-x}$  was estimated to be 48 mol% in the composite. This mole percentage of  $ZrC_xN_{1-x}$  was lower than the total mole percentages of  $ZrC$  and  $ZrN$  in the starting powders (50 mol%). The discrepancy between the nominal eutectic compositions and the compositions that yielded rod-like eutectic structures was probably a consequence of preferential vaporization of  $ZrN$  powder during arc-melting process.<sup>21</sup>

The most commonly observed growth morphologies of eutectic composites were lamellae (alternating parallel platelets of the two eutectic phases) and rods (fibers of one phase distributed continuously in a matrix phase).<sup>22,23</sup> The  $ZrB_2-ZrN$  eutectic composite with a eutectic composition of  $47.5ZrB_2-52.5ZrN_{0.9}$  (mol%) showed a rod-like structure,<sup>13</sup> similar to the structures of the  $ZrB_2-ZrC_xN_{1-x}$  eutectic composites in this study. However, the directionally solidified  $ZrB_2-ZrC$  eutectic composite with a eutectic composition of  $48ZrB_2-52ZrC_{0.9}$  (mol%) was reported to have a lamellar structure.<sup>21</sup> Parisi et al. argued that the lamellar growth was most stable at the eutectic composition, and the spatially periodic structures were stable in a range of spacings, which was limited by dynamical instabilities.<sup>22</sup> A zigzag instability (classical transverse phase diffusion instability) was considered to be the first instability to occur and lead to the breakup of the lamellae into rods or labyrinth structures (depending on the initial spacing and the volume fractions of the eutectic phases).<sup>22</sup> Liu et al. experimentally proved that the lamellar-rod transition could occur over a range of compositions and the instability of a lamella was initiated locally through the formation of a sinusoidal perturbation.<sup>23</sup> In addition, the instabilities in adjacent lamellae were observed to be out of phase, leading to the hexagonal arrangement of the rods during the lamellar to rod transition.<sup>23</sup> It could be noted that the floating zone-melted  $48ZrB_2-52ZrC_{0.9}$  (mol%) eutectic composite prepared by Sorrell et al. was not highly lamellar and a lamellar to rod morphology transition could occur as a consequence of different solidification conditions.<sup>21</sup> The formation of the hexagonally ordered  $ZrC_xN_{1-x}$  rods in this study could be caused by the lamellar to rod transition (driven by the instabilities in adjacent lamellae) as that observed by Liu et al. in the  $Au-Cu$  eutectic system.<sup>23</sup>



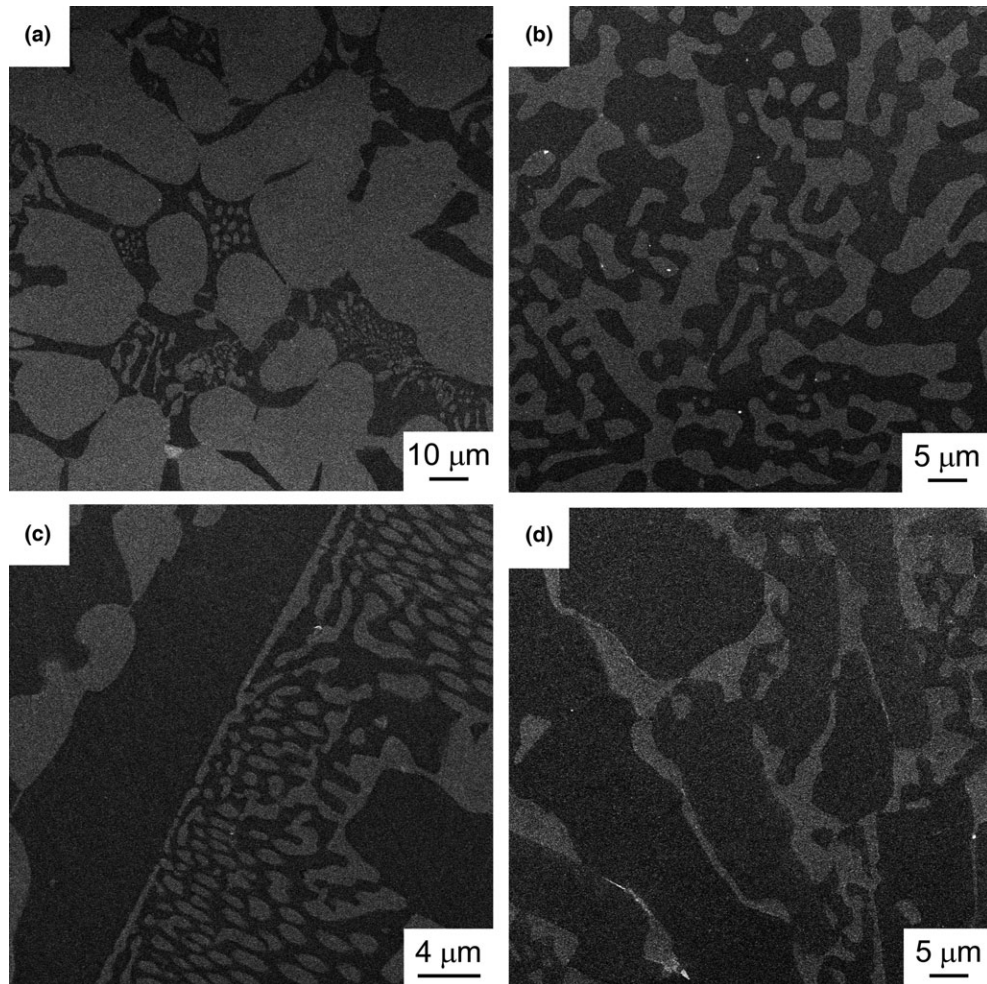


**Fig. 3.** SEM micrographs of the arc-melted ZrB<sub>2</sub>-ZrC-ZrN composites: (a) 30ZrB<sub>2</sub>-50ZrC-20ZrN, (b) 40ZrB<sub>2</sub>-40ZrC-20ZrN, (c) 60ZrB<sub>2</sub>-20ZrC-20ZrN, (d) 80ZrB<sub>2</sub>-10ZrC-10ZrN (mol%).

The instabilities of eutectic growth would vary with solidification parameters. For the intensively studied eutectic ceramic oxide system of Al<sub>2</sub>O<sub>3</sub>-ZrO<sub>2</sub>, a rod-like eutectic structure was formed when prepared by a Bridgman technique,<sup>24</sup> while a lamellar eutectic structure occurred when produced by a high velocity CO<sub>2</sub> laser melting technique.<sup>25</sup>

A backscattered electron SEM micrograph of the 50ZrB<sub>2</sub>-30ZrC-20ZrN (mol%) composite with a rod-like eutectic structure is presented in Fig. 5. There were two contrasts in the micrograph, where the phase with bright contrast was ZrC<sub>x</sub>N<sub>1-x</sub> and the phase with dark contrast was ZrB<sub>2</sub>. EPMA analysis further confirmed that the matrix was ZrB<sub>2</sub> and the dispersoid was ZrC<sub>x</sub>N<sub>1-x</sub>.

Figure 6 presents a bright-field TEM image of the transverse section of the ZrB<sub>2</sub>-ZrC<sub>x</sub>N<sub>1-x</sub> rod-like eutectic structure (a), the corresponding selected-area electron diffraction (SAED) patterns of the ZrC<sub>x</sub>N<sub>1-x</sub> rods (dark phase) (b) and the ZrB<sub>2</sub> matrix (bright phase) (c). No grain boundaries were observed neither in the ZrB<sub>2</sub> matrix nor in the ZrC<sub>x</sub>N<sub>1-x</sub> rods, implying that the ZrC<sub>x</sub>N<sub>1-x</sub> rods were single crystalline and grown in a single-crystalline ZrB<sub>2</sub> matrix. The ZrC<sub>x</sub>N<sub>1-x</sub> rods were hexagonally faceted and the rectilinear boundary of the hexagonal facets corresponded to {211} planes [Fig. 6(a)]. The diffraction patterns shown in Figs. 6(b) and (c) were taken from a specimen at different tilt angles (with several degrees difference). The zone axis of ZrC<sub>x</sub>N<sub>1-x</sub> [111] was almost parallel to that of ZrB<sub>2</sub> [0001]. Sorrell et al. reported that the interfacial orientation relationship in the ZrB<sub>2</sub>-ZrC lamellar eutectic was ZrB<sub>2</sub> (0001)//ZrC (111).<sup>21</sup> In our unpublished work, an in-plane orientation relationship in

the arc-melted ZrB<sub>2</sub>-ZrN rod-like eutectic composite was found to be ZrB<sub>2</sub> (0001)//ZrN (111). The crystal orientation relationship of {111}://{0001} was very common between cubic and hexagonal crystal structures because of the lattice matching.<sup>16,21,26-30</sup> The deviation between the two zone axes of ZrB<sub>2</sub> [0001] and ZrC<sub>x</sub>N<sub>1-x</sub> [111] might be caused by the fluctuation of the eutectic growth conditions. No obvious effect of the ZrC<sub>x</sub>N<sub>1-x</sub> composition on the crystal orientation relationship between the ZrB<sub>2</sub> single-crystalline matrix and the ZrC<sub>x</sub>N<sub>1-x</sub> single-crystalline rods was observed. Figure 7 shows an illustration of the atomic alignment of the ZrC<sub>x</sub>N<sub>1-x</sub> {111} plane along ZrC<sub>x</sub>N<sub>1-x</sub> <111> direction. Since ZrC<sub>x</sub>N<sub>1-x</sub> had a NaCl-type structure, the Zr atoms on the ZrC<sub>x</sub>N<sub>1-x</sub> {111} plane were hexagonally close packed with the hexagonal facet corresponding to {211} plane. This was in consistent with the hexagonally faceted structure of ZrC<sub>x</sub>N<sub>1-x</sub> rods shown in Fig. 6(a).

Figure 8 shows a bright-field TEM image of the longitudinal section of the ZrB<sub>2</sub>-ZrC<sub>x</sub>N<sub>1-x</sub> rod-like eutectic structure (a), the corresponding SAED patterns of the ZrC<sub>x</sub>N<sub>1-x</sub> rods (b) and the interface region between the ZrB<sub>2</sub> matrix and the ZrC<sub>x</sub>N<sub>1-x</sub> rods (c). The single-crystalline ZrC<sub>x</sub>N<sub>1-x</sub> rods were aligned to the growth direction, about 8.5° to the [111] direction. The zone axis of ZrC<sub>x</sub>N<sub>1-x</sub> [101] in Fig. 8(b) was parallel to that of ZrB<sub>2</sub> [2110] in Fig. 8(c). In addition, the ZrC<sub>x</sub>N<sub>1-x</sub> (111) was parallel to ZrB<sub>2</sub> (0220) as indicated in Fig. 8(c). Therefore, the crystal orientation relationship between the single-crystalline ZrB<sub>2</sub> matrix and the single-crystalline ZrC<sub>x</sub>N<sub>1-x</sub> rods in the rod-like eutectic structure was ZrB<sub>2</sub> {0110} // ZrC<sub>x</sub>N<sub>1-x</sub> {111} and ZrB<sub>2</sub> <2110> //

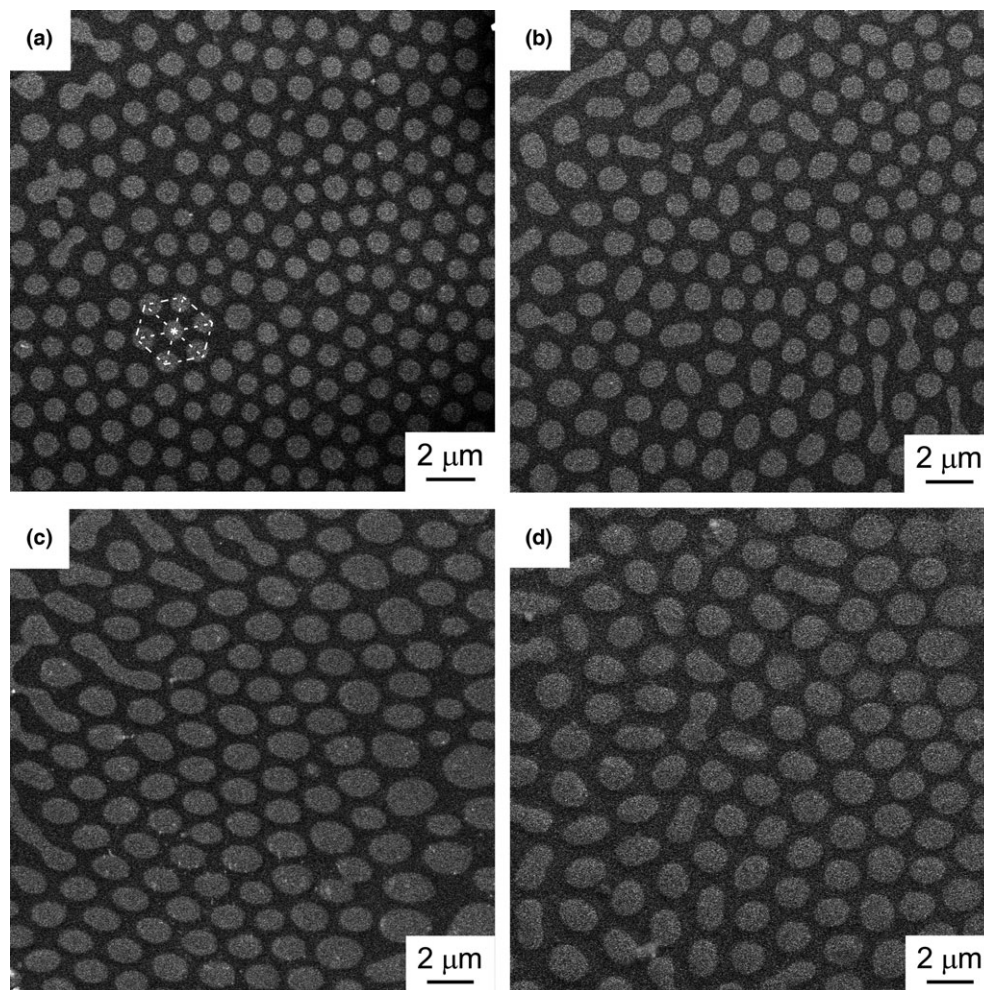


**Fig. 4.** SEM micrographs of the arc-melted  $\text{ZrB}_2$ - $\text{ZrC}$ - $\text{ZrN}$  rod-like eutectic composites: (a) 50 $\text{ZrB}_2$ -10 $\text{ZrC}$ -40 $\text{ZrN}$ , (b) 50 $\text{ZrB}_2$ -25 $\text{ZrC}$ -25 $\text{ZrN}$ , (c) 50 $\text{ZrB}_2$ -30 $\text{ZrC}$ -20 $\text{ZrN}$ , (d) 50 $\text{ZrB}_2$ -40 $\text{ZrC}$ -10 $\text{ZrN}$  (mol%).

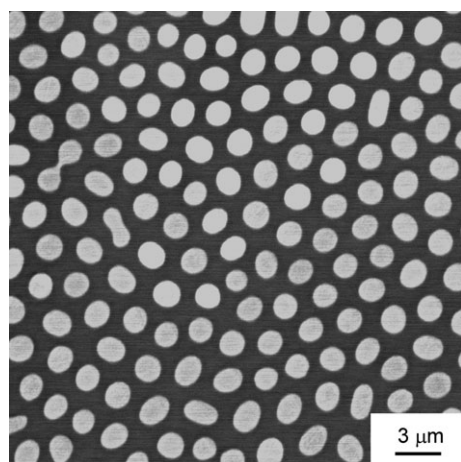


**Fig. 5.** Backscattered electron SEM micrograph of the arc-melted 50 $\text{ZrB}_2$ -30 $\text{ZrC}$ -20 $\text{ZrN}$  composite (mol%).

$\text{ZrC}_x\text{N}_{1-x} <10\bar{1}>$ . However, in the arc-melted  $\text{TiB}_2$ - $\text{TiC}_x\text{N}_{1-x}$  rod-like eutectic structure, a different crystal orientation relationship of  $\text{TiB}_2 <0001>/\text{TiC}_x\text{N}_{1-x} <111>$  and  $\text{TiB}_2 \{11\bar{2}0\}/\text{TiC}_x\text{N}_{1-x} \{202\}$  was observed between the  $\text{TiB}_2$  matrix and the  $\text{TiC}_x\text{N}_{1-x}$  rods.<sup>26</sup> The crystal orientation relationship between phases in the floating zone-melted  $\text{ZrB}_2$ - $\text{ZrC}$  lamellar eutectic structure was  $\text{ZrB}_2 <\bar{1}210>/\text{ZrC} <01\bar{1}>$  and  $\text{ZrB}_2 \{0001\}/\text{ZrC} \{111\}$ , which was the same as that found in the arc-melted  $\text{TiB}_2$ - $\text{TiC}_x\text{N}_{1-x}$  rod-like

eutectic structure.<sup>21,26</sup> As shown in Fig. 8, the growth direction of the  $\text{ZrC}_x\text{N}_{1-x}$  rods was close to  $\text{ZrC}_x\text{N}_{1-x} [1\bar{1}1]$  and the angle between  $\text{ZrB}_2 [0001]$  and  $\text{ZrC}_x\text{N}_{1-x} [1\bar{1}1]$  was about  $20^\circ$ . The eutectic growth direction shown in Fig. 8 was different from that depicted in Fig. 6, where  $\text{ZrB}_2 [0001]$  was almost parallel to  $\text{ZrC}_x\text{N}_{1-x} [111]$ . Therefore, there were multiple crystal orientation relationships between the  $\text{ZrB}_2$  matrix and the  $\text{ZrC}_x\text{N}_{1-x}$  rods. Fig. 9(a) presents a bright-field TEM image of the end of a  $\text{ZrC}_x\text{N}_{1-x}$  rod and Fig. 9(b) depicts a high-resolution TEM image of the designated area b in Fig. 9(a). The interface between  $\text{ZrB}_2$  and  $\text{ZrC}_x\text{N}_{1-x}$  was wavy and clean, and no impurity phases were observed.

The dependence of the Vickers hardness of the arc-melted  $\text{ZrB}_2$ - $\text{ZrC}$ - $\text{ZrN}$  composites on  $\text{ZrB}_2$  content ( $\text{ZrC}/\text{ZrN} = 1:1$ ) is depicted in Fig. 10. The applied indentation loads were 2 and 5 N, respectively. The  $H_V$  increased first and then decreased with increasing  $\text{ZrB}_2$  content. It reached the maximum at  $\text{ZrB}_2$  content of 50 mol%. The 50 $\text{ZrB}_2$ -25 $\text{ZrC}$ -25 $\text{ZrN}$  composite with a rod-like eutectic structure showed the highest  $H_V$  value of 18.6 GPa (indentation load: 2 N). The hardening effect could be attributed to the small grain size of the rod-like eutectic structure. The hardness of 2 N indentation was higher than that of 5 N indentation, but they showed similar trend with increasing  $\text{ZrB}_2$  content. The  $H_V$  value of the  $\text{ZrB}_2$ - $\text{ZrC}_x\text{N}_{1-x}$  composites was lower than that of a dense  $\text{ZrB}_2$ - $\text{ZrC}_x$  composite (about 20 GPa at indentation load of 5 N) produced by reactive hot-pressing, because the grain sizes of the  $\text{ZrB}_2$  and  $\text{ZrC}_x$  were much smaller (about 0.6 and 0.4  $\mu\text{m}$ , respectively) than that of  $\text{ZrB}_2$  and  $\text{ZrC}_x\text{N}_{1-x}$  in this study.<sup>31</sup> Another reason for the



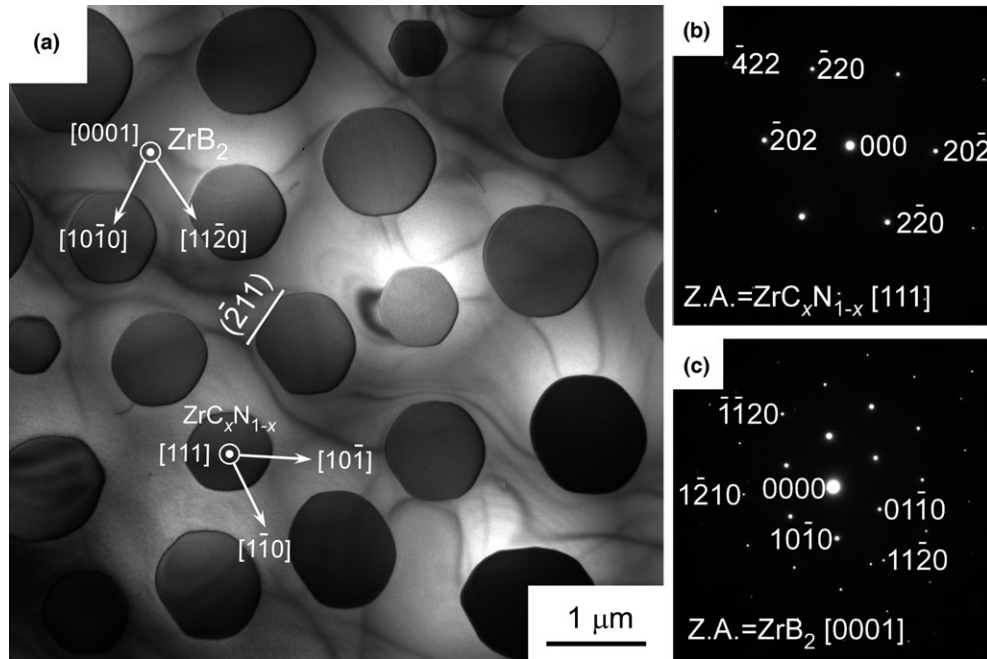


**Fig. 6.** Bright-field TEM image of the transverse section of the ZrB<sub>2</sub>-ZrC<sub>x</sub>N<sub>1-x</sub> rod-like eutectic structure (a); SAED pattern of the ZrC<sub>x</sub>N<sub>1-x</sub> rods (b); SAED pattern of the ZrB<sub>2</sub> matrix (c). The diffraction patterns shown in (b) and (c) were taken from a sample at different tilt angles (with several degrees difference).

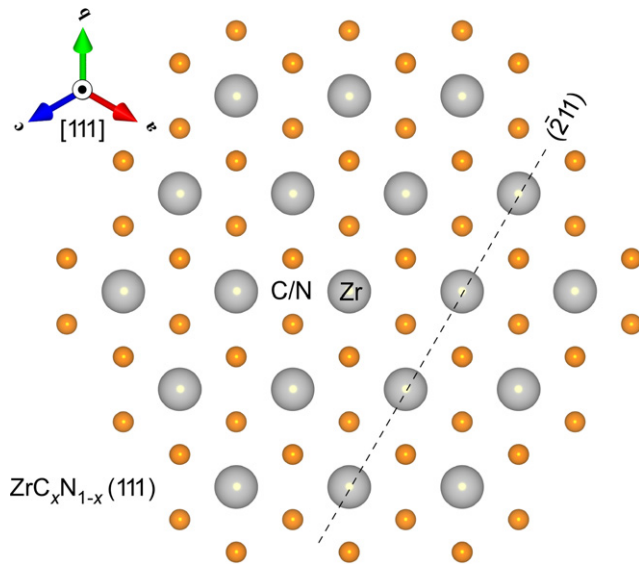


**Fig. 7.** Illustration of the atomic alignment of ZrC<sub>x</sub>N<sub>1-x</sub> {111} lattice plane along ZrC<sub>x</sub>N<sub>1-x</sub> <111> direction.

discrepancy was that ZrB<sub>2</sub> and ZrC were reported to be harder than ZrN.<sup>12,13,32</sup> The hardness of the directionally solidified ZrB<sub>2</sub>-ZrC lamellar eutectics were reported to have a maximum Knoop hardness of 24 GPa at an indentation load of 4.9 N.<sup>10</sup> The hardness of the ZrB<sub>2</sub>-ZrC lamellar eutectics exhibited the classical Hall-Petch behavior with interlamellar spacing in the range of 1.85 to 2.75 μm.<sup>10</sup> However, it was difficult to compare Knoop hardness with Vickers hardness due to the different propensities for cracking, and different sensitivities to load and indenter geometry.<sup>33</sup> A concomitant increase in Vickers hardness with decreasing microstructural scale, a near-linear relationship rather than a traditional Hall-Petch relationship, was observed in a laser irradiation-produced B<sub>4</sub>C-TiB<sub>2</sub> lamellar eutectic ceramic composite, which reached a high Vickers hardness of 32 GPa (indentation load: 9.81 N) at an interlamellar spacing of 0.18 μm.<sup>34</sup>

The Vickers hardness of the rod-like eutectic composites with 50 mol% ZrB<sub>2</sub> increased slightly with increasing C/N ratio as shown in Fig. 11. As mentioned above, the diameter of the ZrC<sub>x</sub>N<sub>1-x</sub> rods slightly increased with increasing C/N ratio. Classically, a decrease in Vickers hardness value would be expected for larger grain sizes according to the Hall-Petch equation.<sup>35</sup> The hardness of the ZrB<sub>2</sub> matrix would not change with the ZrC<sub>x</sub>N<sub>1-x</sub> fractions. Thus, the increase in hardness with composition was due to the increase in hardness from the solid solution of ZrC<sub>x</sub>N<sub>1-x</sub> phase. The hardness of ZrC<sub>x</sub>N<sub>1-x</sub> would increase with the *x* value since ZrC had a higher hardness than ZrN.<sup>12,13</sup> The evolution of the hardness of the rod-like eutectic composites with 50 mol% ZrB<sub>2</sub> could be the result of two competing mechanisms: the Hall-Petch relationship and rule-of-mixtures law, and generally followed a rule-of-mixtures type of behavior.

Figure 12 shows the load dependence of the Vickers hardness of the 50ZrB<sub>2</sub>-50ZrC<sub>x</sub>N<sub>1-x</sub> (the tested composite was 50ZrB<sub>2</sub>-40ZrC-10ZrN) eutectic composite. At indentation loads less than 10 N, the Vickers hardness was load dependent and decreased linearly with increasing applied load. At indentation loads greater than 10 N, the Vickers hardness became constant with an abrupt transition to a constant value about 15 GPa. Low indentation loads were associated with deformation, whereas fracture was more prominent at high indentation loads, in which the cracking might influence the hardness of one material that had cracked.<sup>35</sup> Similarly, a plateau in the hardness-load curve was observed in the laser-processed B<sub>4</sub>C-TiB<sub>2</sub> lamellar eutectic composite with an interlamellar spacing of 0.35 μm.<sup>34</sup> The Vickers hardness-load curves for typical brittle ceramics, such as Al<sub>2</sub>O<sub>3</sub>, Si<sub>3</sub>N<sub>4</sub>, and α-SiC, also exhibited a distinct transition to a plateau hardness level that corresponded to a relationship among hardness, Young's modulus, and fracture toughness.<sup>33</sup>

#### IV. Conclusions

ZrB<sub>2</sub>-ZrC<sub>x</sub>N<sub>1-x</sub> quasi-binary eutectic composites were prepared by arc-melting ZrB<sub>2</sub>, ZrC, and ZrN powders in an N<sub>2</sub> atmosphere. The composites had only ZrB<sub>2</sub> and ZrC<sub>x</sub>N<sub>1-x</sub> two phases and showed a rod-like eutectic structure at a

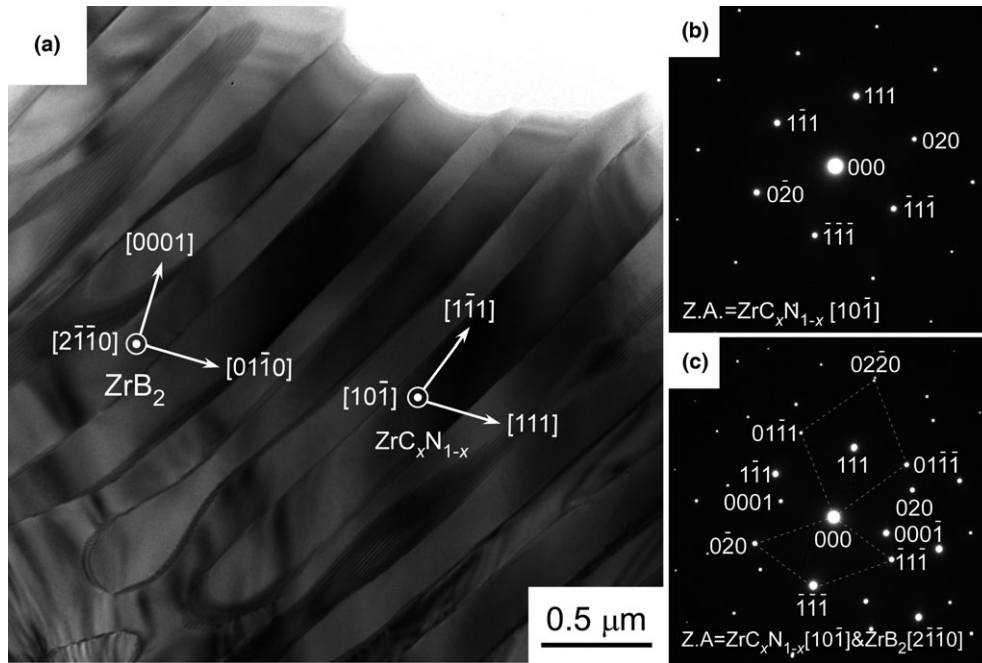


Fig. 8. Bright-field TEM image of the longitudinal section of the ZrB<sub>2</sub>-ZrC<sub>x</sub>N<sub>1-x</sub> rod-like eutectic structure (a); SAED pattern of the ZrC<sub>x</sub>N<sub>1-x</sub> rods (b); SAED pattern of the interface region between the ZrB<sub>2</sub> matrix and the ZrC<sub>x</sub>N<sub>1-x</sub> rod (c).

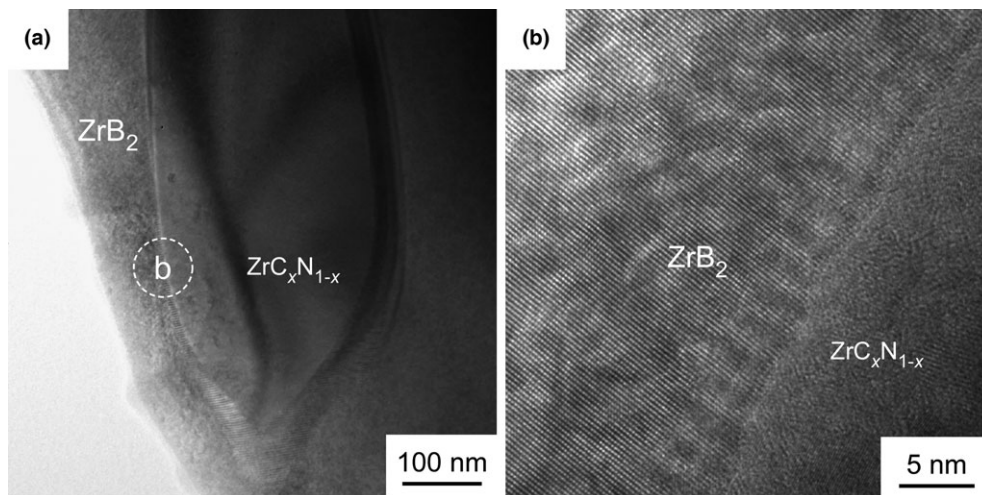


Fig. 9. (a) Bright-field TEM image of the end of a ZrC<sub>x</sub>N<sub>1-x</sub> rod; (b) high-resolution TEM image of the designated area b in (a).

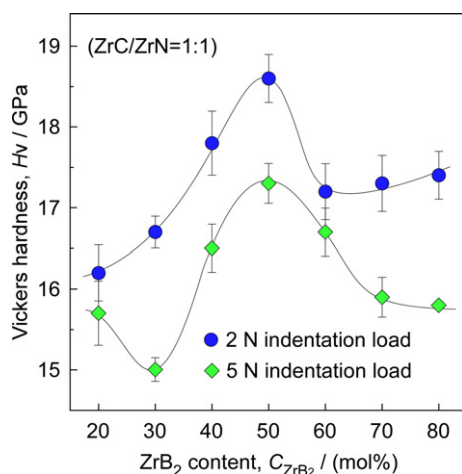


Fig. 10. Dependence of the Vickers hardness of the arc-melted ZrB<sub>2</sub>-ZrC-ZrN composites on ZrB<sub>2</sub> content (ZrC/ZrN = 1:1, indentation loads: 2 N and 5 N, respectively).

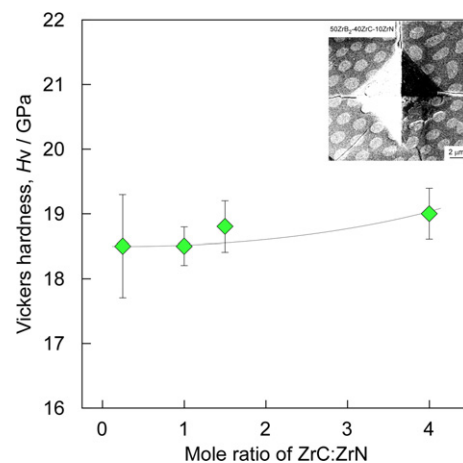


Fig. 11. Dependence of the Vickers hardness of the 50ZrB<sub>2</sub>-50ZrC<sub>x</sub>N<sub>1-x</sub> (mol%) composites on C/N ratio (indentation load: 2 N; the inset of Fig. 11 showing the top view of an indentation impression of 50ZrB<sub>2</sub>-40ZrC-10ZrN (mol%) composite).

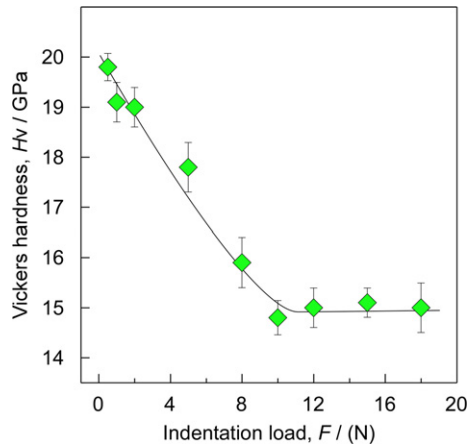


Fig. 12. Load dependence of the Vickers hardness of the 50ZrB<sub>2</sub>-50ZrC<sub>x</sub>N<sub>1-x</sub> (mol%) composites.

nominal composition of 50 mol% of ZrB<sub>2</sub>, irrespective of the ZrC/ZrN ratio. In the ZrB<sub>2</sub>-ZrC<sub>x</sub>N<sub>1-x</sub> rod-like eutectic structures, single-crystalline ZrC<sub>x</sub>N<sub>1-x</sub> rods were grown in single-crystalline ZrB<sub>2</sub> matrices. Of the two crystal orientation relationships observed between phases in the ZrB<sub>2</sub>-ZrC<sub>x</sub>N<sub>1-x</sub> eutectic composites, one was determined as ZrB<sub>2</sub> {0110} // ZrC<sub>x</sub>N<sub>1-x</sub> {111} and ZrB<sub>2</sub> <2110> // ZrC<sub>x</sub>N<sub>1-x</sub> <101>. The Vickers hardness of the ZrB<sub>2</sub>-ZrC<sub>x</sub>N<sub>1-x</sub> rod-like eutectic composite was load dependant at low indentation loads (less than 10 N) and was higher than that of the hypo- and hypereutectic composites. The 50ZrB<sub>2</sub>-40ZrC-10ZrN (mol%) eutectic composite showed the highest Vickers hardness of 19 GPa at an indentation load of 2 N.

### Acknowledgment

This study was supported by the Tohoku University, Japan and the MEXT (Ministry of Education, Culture, Sports, Science and Technology), Scientific Research (B) No. 25289223. Eric Jianfeng Cheng thanks the financial support from the China Scholarship Council, P.R.China. Eric Jianfeng Cheng would also thank Dr. Robert Schmidt for proofreading the manuscript.

### References

- E. Wuchina, E. Opila, M. Opeka, W. Fahrenholtz, and I. Talmy, "UHTCs: Ultra-High Temperature Ceramic Materials for Extreme Environment Applications," *Electrochem. Soc. Interface*, **16** [4] 30-6 (2007).
- W. G. Fahrenholtz, G. E. Hilmas, I. G. Talmy, and J. A. Zaykoski, "Refractory Diborides of Zirconium and Hafnium," *J. Am. Ceram. Soc.*, **90** [5] 1347-64 (2007).
- M. W. Bird, T. Rampton, D. Fullwood, P. F. Becher, and K. W. White, "Local Dislocation Creep Accommodation of a Zirconium Diboride Silicon Carbide Composite," *Acta Mater.*, **84** [0] 359-67 (2015).
- V. Medri, F. Monteverde, A. Balbo, and A. Bellosi, "Comparison of ZrB<sub>2</sub>-ZrC-SiC Composites Fabricated by Spark Plasma Sintering and Hot Pressing," *Adv. Eng. Mater.*, **7** [3] 159-63 (2005).
- J. Adachi, K. Kurosaki, M. Uno, and S. Yamanaka, "Porosity Influence on the Mechanical Properties of Polycrystalline Zirconium Nitride Ceramics," *J. Nucl. Mater.*, **358** [2-3] 106-10 (2006).
- M. F. Ashby, "Criteria for Selecting the Components of Composites," *Acta Metall. Mater.*, **41** [5] 1313-35 (1993).
- A. Sayir and S. C. Farmer, "The Effect of the Microstructure on Mechanical Properties of Directionally Solidified Al<sub>2</sub>O<sub>3</sub>/ZrO<sub>2</sub>(Y<sub>2</sub>O<sub>3</sub>) Eutectic," *Acta Mater.*, **48** [18-19] 4691-7 (2000).
- Y. Waku, N. Nakagawa, T. Wakamoto, H. Ohtsubo, K. Shimizu, and Y. Kohtoku, "High-Temperature Strength and Thermal Stability of a Unidirectionally Solidified Al<sub>2</sub>O<sub>3</sub>/YAG Eutectic Composite," *J. Mater. Sci.*, **33** [5] 1217-25 (1998).
- Y. Waku, N. Nakagawa, T. Wakamoto, H. Ohtsubo, K. Shimizu, and Y. Kohtoku, "A Ductile Ceramic Eutectic Composite with High Strength at 1,873 K," *Nature*, **389** [6646] 49-52 (1997).
- C. C. Sorrell, V. S. Stubican, and R. C. Bradt, "Mechanical Properties of ZrC-ZrB<sub>2</sub> and ZrC-TiB<sub>2</sub> Directionally Solidified Eutectics," *J. Am. Ceram. Soc.*, **69** [4] 317-21 (1986).
- C. M. Chen, L. T. Zhang, W. C. Zhou, Z. Z. Hao, Y. J. Jiang, and S. L. Yang, "Microstructure, Mechanical Performance and Oxidation Mechanism of Boride In Situ Composites," *Compos. Sci. Technol.*, **61** [7] 971-5 (2001).
- S. S. Ordanyan and V. I. Unrod, "Reactions in the System ZrC-ZrB<sub>2</sub>," *Sov. Powder Metall.*, **14** [5] 393-5 (1975).
- S. S. Ordanyan and V. D. Chupov, "Interaction in ZrN-ZrB<sub>2</sub> and HfN-HfB<sub>2</sub> Systems," *Inorg. Mater.*, **20** [12] 1719-22 (1985).
- I. Danisina, R. Avarbe, Y. A. Omel'chenko, and T. Ryzhkova, "Phase Diagram of the System Zirconium-Zirconium Nitride-Zirconium Carbide," *Zh. Prikl. Khim.*, **41**, 492-500 (1968).
- E. J. Cheng, H. Katsui, R. Tu, and T. Goto, "Rod-Like Eutectic Structure of arc-Melted TiB<sub>2</sub>-TiC<sub>x</sub>N<sub>1-x</sub> Composite," *J. Eur. Ceram. Soc.*, **34** [9] 2089-94 (2014).
- D. Vallauri, I. Adrián, and A. Chrysanthou, "TiC-TiB<sub>2</sub> Composites: A Review of Phase Relationships, Processing and Properties," *J. Eur. Ceram. Soc.*, **28** [8] 1697-713 (2008).
- E. J. F. Cheng, H. Katsui, and T. Goto, "Lamellar and Rod-Like Eutectic Growth of TiB<sub>2</sub>-TiC-TiN Composites by Arc-Melting"; pp. 43-6 in *Key Engineering Materials*, Vol. 616, pp. 43-6 Trans Tech Publications Ltd., Switzerland, 2014.
- K. Momma and F. Izumi, "VESTA: A Three-Dimensional Visualization System for Electronic and Structural Analysis," *J. Appl. Crystallogr.*, **41** [3] 653-8 (2008).
- K. Nakamura and M. Yashima, "Crystal Structure of NaCl-Type Transition Metal Monocarbides MC (M = V, Ti, Nb, Ta, Hf, Zr), a Neutron Powder Diffraction Study," *Mater. Sci. Eng., B*, **148** [1] 69-72 (2008).
- K. Aigner, W. Lengauer, D. Rafaja, and P. Ettmayer, "Lattice Parameters and Thermal Expansion of Ti (C<sub>x</sub>N<sub>1-x</sub>), Zr (C<sub>x</sub>N<sub>1-x</sub>), Hf (C<sub>x</sub>N<sub>1-x</sub>) and TiN<sub>1-x</sub> from 298 to 1473 K as Investigated by High-Temperature X-ray Diffraction," *J. Alloys. Compd.*, **215**, 121-6 (1994).
- C. Sorrell, H. Beratan, R. Bradt, and V. Stubican, "Directional Solidification of (Ti, Zr) Carbide-(Ti, Zr) Diboride Eutectics," *J. Am. Ceram. Soc.*, **67** [3] 190-4 (1984).
- A. Parisi and M. Plapp, "Stability of Lamellar Eutectic Growth," *Acta Mater.*, **56** [6] 1348-57 (2008).
- S. Liu, J. H. Lee, and R. Trivedi, "Dynamic Effects in the Lamellar-Rod Eutectic Transition," *Acta Mater.*, **59** [8] 3102-15 (2011).
- F. Schmid and D. Viehnicki, "Oriented Eutectic Microstructures in the System Al<sub>2</sub>O<sub>3</sub>/ZrO<sub>2</sub>," *J. Mater. Sci.*, **5** [6] 470-3 (1970).
- S. Bourban, N. Karapatis, H. Hofmann, and W. Kurz, "Solidification Microstructure of Laser Remelted Al<sub>2</sub>O<sub>3</sub>-ZrO<sub>2</sub> Eutectic," *Acta Mater.*, **45** [12] 5069-75 (1997).
- E. J. Cheng, H. Katsui, R. Tu, and T. Goto, "Long-Range Ordered Structure of Ti-B-C-N in a TiB<sub>2</sub>-TiC<sub>x</sub>N<sub>1-x</sub> Eutectic Composite," *J. Am. Ceram. Soc.*, **97** [8] 2423-6 (2014).
- J. Y. Dai, Y. G. Wang, D. X. Li, and H. Q. Ye, "Atomic Structure at Ti (C,N)-TiB<sub>2</sub> Interfaces in Ti(C,N)-TiB<sub>2</sub>-Ni Ceramics," *Philos. Mag. A*, **70** [5] 905-16 (1994).
- F. Mei, N. Shao, L. Wei, Y. Dong, and G. Li, "Coherent Epitaxial Growth and Superhardness Effects of c-TiN/h-TiB<sub>2</sub> Nanomultilayers," *Appl. Phys. Lett.*, **87** [1] 011906-9 (2005).
- J. Y. Dai, D. X. Li, H. Q. Ye, G. J. Zhang, and Z. Z. Jin, "Characterization of TiB<sub>2</sub>-Ti(CN)-Ni Ceramics by Transmission and Analytical Electron Microscopy," *Mater. Lett.*, **16** [6] 317-21 (1993).
- H. Holleck, C. Kühn, and H. Schulz, "Wear Resistant Carbide-Boride Composite Coatings," *J. Vac. Sci. Technol., A*, **3** [6] 2345-7 (1985).
- L. Rangaraj, S. J. Suresha, C. Divakar, and V. Jayaram, "Low-Temperature Processing of ZrB<sub>2</sub>-ZrC Composites by Reactive Hot Pressing," *Metall. Mater. Trans. A*, **39** [7] 1496-505 (2008).
- C. Chen, C. Liu, and C. Y. A. Tsao, "Influence of Growth Temperature on Microstructure and Mechanical Properties of Nanocrystalline Zirconium Carbide Films," *Thin Solid Films*, **479** [1-2] 130-6 (2005).
- J. Quinn and G. D. Quinn, "Indentation Brittleness of Ceramics: A Fresh Approach," *J. Mater. Sci.*, **32** [16] 4331-46 (1997).
- R. M. White, J. M. Kunkle, A. V. Polotai, and E. C. Dickey, "Microstructure and Hardness Scaling in Laser-Processed B<sub>4</sub>C-TiB<sub>2</sub> Eutectic Ceramics," *J. Eur. Ceram. Soc.*, **31** [7] 1227-32 (2011).
- E. Hall, "The Deformation and Ageing of Mild Steel: III Discussion of Results," *Proc. Phys. Soc. London, Sect. B*, **64** [9] 747-53 (1951). □